PNAS RESEARCH ARTICLE | MICROBIOLOGY

Biofilm formation by *Staphylococcus aureus* is triggered by a drop in the levels of a cyclic dinucleotide

Adnan K. Syed[a,1,2], Rishika Baral[b,1], Erik R. Van Vlack[c,3], María Luisa Gil-Marqués[d], Taliesin Lenhart[a,4], David C. Hooper[d], Daniel Kahne[c], Richard Losick[a,5], and Niels Bradshaw[b,5]

Affiliations are included on p. 10.

Contributed by Richard Losick; received August 26, 2024; accepted November 11, 2024; reviewed by Angelika Grundling and Alexander R. Horswill

The bacterial pathogen *Staphylococcus aureus* forms multicellular communities known as biofilms in which cells are held together by an extracellular matrix principally composed of repurposed cytoplasmic proteins and extracellular DNA. These biofilms assemble during infections or under laboratory conditions by growth on medium containing glucose, but the intracellular signal for biofilm formation and its downstream targets were unknown. Here, we present evidence that biofilm formation is triggered by a drop in the levels of the second messenger cyclic-di-AMP. Previous work identified genes needed for the release of extracellular DNA, including genes for the cyclic-di-AMP phosphodiesterase GdpP, the transcriptional regulator XdrA, and the purine salvage enzyme Apt. Using a cyclic-di-AMP riboswitch biosensor and mass spectrometry, we show that the second messenger drops in abundance during biofilm formation in a glucose-dependent manner. Mutation of these three genes elevates cyclic-di-AMP and prevents biofilm formation in a murine catheter model. Supporting the generality of this mechanism, we found that *gdpP* was required for biofilm formation by diverse strains of *S. aureus*. We additionally show that the downstream consequence of the drop in cyclic-di-AMP is inhibition of the "accessory gene regulator" operon *agr*, which is known to suppress biofilm formation through phosphorylation of the transcriptional regulator AgrA by the histidine kinase AgrC. Consistent with this, an *agr* mutation bypasses the block in biofilm formation and eDNA release caused by a *gdpP* mutation. Finally, we report the unexpected observation that GdpP inhibits phosphotransfer from AgrC to AgrA, revealing a direct connection between the phosphodiesterase and *agr*.

biofilm formation | cyclic-di-AMP | *Staphylococcus aureus*

Significance

Bacteria form multicellular communities known as biofilms, which are held together by an extracellular matrix. The pathogen *Staphylococcus aureus* forms biofilms in which cells are held together by a matrix consisting of protein and DNA. Evidence is presented that biofilm formation is triggered by a drop in the levels of a second messenger, cyclic-di-adenosine monophosphate, that depends on the phosphodiesterase GdpP. Evidence also indicates that the drop in the levels of the second messenger acts by inhibiting a multigene regulatory system known as the "accessory gene regulator" operon *agr*, which is known to suppress biofilm formation through phosphorylation of the transcriptional regulator AgrA by the kinase AgrC. GdpP could be an attractive target for therapeutic agents that block biofilm formation.

Biofilms are microbial communities in which cells adhere to each other by means of an extracellular matrix composed of DNA, proteins, and/or polysaccharides. These matrix components are produced by the microbes in the community either through dedicated pathways, as in the cases of curli and cellulose production in *Escherichia coli* and TasA and the EPS exopolysaccharide in *Bacillus subtilis*, or through lysis of a subset of cells and recycling of cytoplasmic components, as in the cases of *Pseudomonas aeruginosa* and *Staphylococcus aureus* (1–11). The biofilm state confers resistance to a variety of assaults including from predators, competitors, and the immune system (12–16). Biofilm formation often also plays an essential role in recalcitrant infections by contributing to antibiotic tolerance and evasion of immune cells (17, 18). In the case of *S. aureus* therapeutic approaches to disrupt biofilms represent a significant unmet need.

The matrix of *S. aureus* biofilms is composed of extracellular DNA, proteins, and polysaccharide. The best understood matrix component is the secreted exopolysaccharide, known as polysaccharide intercellular adhesin (PIA), which is produced by the *ica* operon (19). While PIA is required for biofilm formation by some *S. aureus* strains, particularly methicillin-sensitive strains (MSSA), it is dispensable in many other strains, particularly methicillin-resistant strains (MRSA) (11, 20). In contrast, the extracellular DNA and protein components of the biofilm matrix appear to be widely required. Thus, we focus here on how these components are supplied to the matrix and whether there are mechanistic commonalities across *S. aureus* strains.

Several recent studies have indicated that the principal proteins found in the biofilm are cytoplasmic proteins that are released from cells during biofilm formation to moonlight as matrix proteins (1, 3, 11, 21). These major matrix proteins contrast with dedicated factors that adhere cells to surfaces and promote formation of small clumps of cells at early stages of biofilm formation. The matrix proteins, which are positively charged at the low pH at which biofilm formation takes place (e.g., fermentation during growth on medium containing glucose), associate with the negatively charged cell surface (11).

Reviewers: A.G., Imperial College London; and A.R.H., University of Colorado Anschutz Medical Campus.

The authors declare no competing interest.

[1]A.K.S. and R.B. contributed equally to this work.

[2]Present address: Breaking, Inc., Boston, MA 02109.

[3]Present address: Generate Biomedicines, Somerville, MA 02143.

[4]Present address: Division of Pathology, Cincinnati Children's Hospital, Cincinnati, OH 45229.

[5]To whom correspondence may be addressed. Email: losick@mcb.harvard.edu or niels@brandeis.edu.

This article contains supporting information online at https://www.pnas.org/lookup/suppl/doi:10.1073/pnas.2417323121/-/DCSupplemental.

Published December 16, 2024.

Notably, these glucose-dependent biofilms have properties that are similar to biofilms formed in infections but are distinct from communities formed under other conditions (for example high salt) that are highly dependent on adhesion factors.

Evidence indicates that the DNA component of the matrix is chromosomal DNA (referred to as extracellular DNA or eDNA) that has been repurposed as in the case of the matrix proteins. The eDNA forms an electrostatic net with the protein-coated cells holding them together (2, 22–24). Whether there is a common trigger for biofilm formation and/or a requirement for eDNA that is shared across *S. aureus* strains is not known (1).

Using a comprehensive and unbiased genome-wide transposon sequencing approach, we previously identified several genes that are required for the release of eDNA from a strain of *S. aureus* cells during glucose-dependent biofilm formation (25). Among these were *gdpP*, which encodes the cyclic-di-AMP (c-di-AMP) phosphodiesterase GdpP, *xdrA*, which specifies the transcription regulatory protein XdrA, and *apt*, the gene for the adenine phosphoribosyltransferase Apt. Mutants of all three genes exhibited marked defects in the release of eDNA and biofilm formation. Analysis using HPLC showed that the levels of c-di-AMP decreased during growth of the wild type on biofilm-inducing medium [Tryptone Soy Broth (TSB) containing glucose] whereas the levels rose in cells mutant for GdpP. These findings raised the possibility that biofilm formation in *S. aureus* is triggered by a drop in c-di-AMP levels.

Here, we present evidence in support of this hypothesis and report on the mechanism by which c-di-AMP acts. Previous studies had implicated the quorum-sensing system encoded by the "accessory gene regulon" *agr* operon as being a negative regulator of biofilm formation and eDNA release and is also involved in promoting biofilm dispersal (26, 27). Whether *agr* and c-di-AMP control mechanisms were related was not known. Importantly, we show that c-di-AMP controls the activity of the upstream member of this system, the histidine kinase AgrC, which inhibits biofilm formation through phosphorylating and activating the transcription factor AgrA (28, 29). Additionally, we present evidence for the unexpected finding that GdpP inhibits the phosphotransferase activity of AgrC and speculate on its role in the pathway governing biofilm formation.

Results

eDNA Release Is a Common Feature of Biofilm Formation. Because biofilm formation has been studied in a variety of strains, we began by asking whether eDNA release is a common feature of biofilm formation by *S. aureus*. Accordingly, we investigated biofilm formation using four strains (HG003, SH1000, MN8, RN1) that are known to form glucose-dependent biofilms (30–34). All of these strains formed robust biofilms in our hands and did so in a glucose-dependent manner (Fig. 1*A*). Moreover, as judged by light microscopy all these strains formed large clumps of cells (*SI Appendix*, Fig. S1). Also, all four strains released eDNA release during biofilm formation, and the integrity of the resulting biofilms was dependent on the eDNA in that the biofilms and cell clumps were substantially dispersed by treatment with the enzyme DNase I (Fig. 1*A* and *SI Appendix*, Fig. S1).

It should be noted that RN1, HG003, and SH1000 are related strains that have been repaired for important *S. aureus* regulatory factors; HG003 was derived from the RN1 strain by repair of mutations in *rsbU* and *tcaR*, whereas SH1000 was derived from RN1 by repair of mutation in *rsbU* and cured of phage (34). Thus, the global regulators *rsbU* and *tcaR* are not required for *gdpP*- and eDNA-dependent biofilm formation. Strengthening the argument

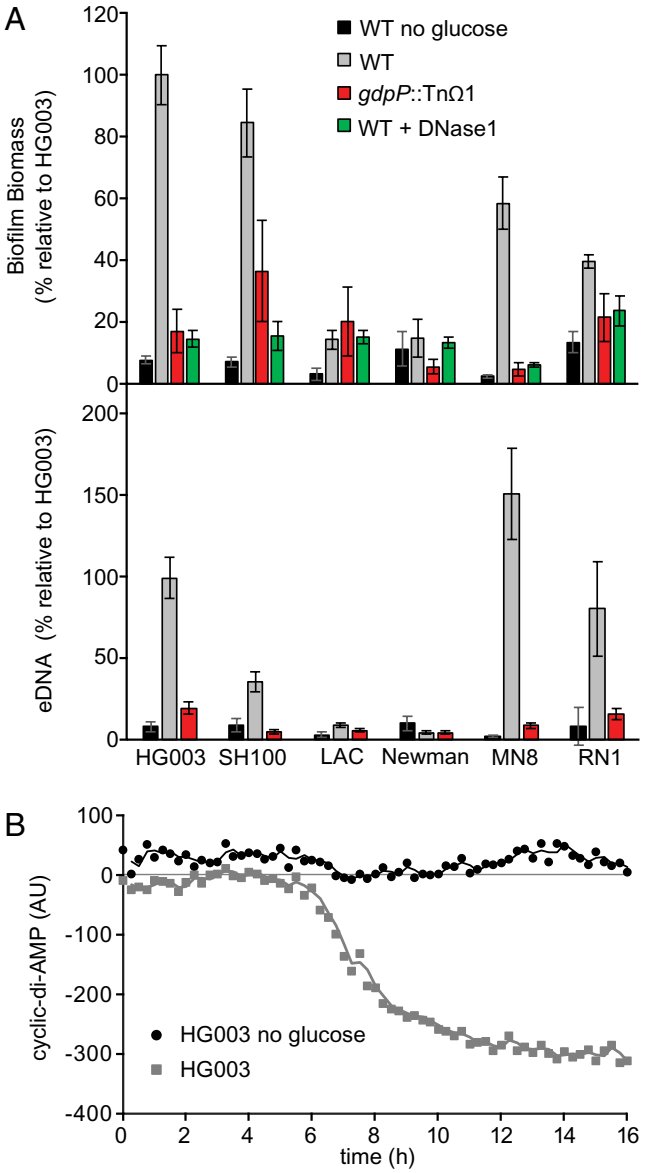

Fig. 1. eDNA release and dependence on *gdpP* is a shared feature of biofilm formation by multiple strains of *S. aureus*. (*A*) The indicated strains were tested for their ability to form glucose- and DNA-dependent biofilms (*Top*) and to release eDNA (*Bottom*). *gdpP*::TnΩ1 (red) was transduced into each strain and the mutant strains were tested for their ability to form glucose-dependent (*Top*) biofilms and release eDNA (*Bottom*). DNase I was added to established biofilms for 1 h prior to harvesting to test the dependence on DNA (green). (*B*) Cells containing a cyclic-di-AMP sensitive riboswitch biosensor were grown under conditions that do not permit biofilm formation (no added glucose, black) or biofilm promoting conditions (plus glucose, gray). Cyclic-di-AMP levels dropped between 6 and 8 h in a glucose-dependent manner.

that the mechanism of biofilm formation is broadly conserved, the USA200 type strain MN8 is from a different lineage than the other strains. In contrast, and as has been reported, two other strains, USA300 LAC (which expresses a nuclease that weakens biofilms) (23) and Newman, were relatively unresponsive to growth on glucose and did not form robust biofilms as judged by eDNA release and biofilm mass in our hands (2). We conclude that eDNA release and dependence on eDNA for biofilm formation and integrity are characteristic of strains that form robust biofilms in a glucose-dependent manner.

Of special interest were the results with strain MN8 as this strain is known to produce biofilms in a manner that depends on the exopolysaccharide PIA (35). Still, in our hands, MN8 was

found to release eDNA during biofilm formation and the integrity of the resulting biofilms was strongly dependent on eDNA (Fig. 1*A*).

Dependence on the c-di-AMP Phosphodiesterase GdpP Is a General Feature of eDNA Release during Biofilm Formation. Our previous work has shown that in strain HG003, eDNA release during biofilm formation and biofilm formation itself are significantly impaired by mutation of the gene for the c-di-AMP phosphodiesterase *gdpP* (25). To investigate whether this is generally the case, we transduced the transposon insertion *gdpP*::TnΩ1 from HG003 into SH1000, RN1, and MN8. All four strains exhibited a marked decrease in eDNA release, biofilm formation, and cell clumping when the *gdpP* mutation was introduced (Fig. 1*A* and *SI Appendix*, Fig. S1). These data are consistent with our hypothesis that dependence on *gdpP* for the release of eDNA is a common feature of biofilm forming strains of *S. aureus*. Henceforth we will focus on HG003 and its mutant derivatives.

c-di-AMP Levels Drop during Biofilm Formation. Previously, using HPLC, we found that c-di-AMP levels were lower in biofilm cells than in cells grown in the absence of glucose, leading to the hypothesis that eDNA release and biofilm formation are triggered by a drop in the levels of the second messenger (25). To facilitate further tests of this hypothesis, we turned to the use of a riboswitch reporter for c-di-AMP created, and kindly provided to us, by Ming Hammond (36). The riboswitch is attached to a Spinach2 aptamer that binds to a dye that fluoresces when the riboswitch is bound by c-di-AMP, allowing a fluorescence readout of relative changes in c-di-AMP levels in living cells over time. In keeping with our previous observations, we observed a glucose-dependent drop in c-di-AMP levels commencing at 6 to 8 h after inoculation and persisting for the duration of the experiment (Fig. 1*B*). In contrast, cells grown in TSB medium without added glucose showed little to no change in the level of c-di-AMP during the course of the experiment (Fig. 1*B*). HPLC-mass spectrometry was used to verify that the level of c-di-AMP did decrease in response to growth on glucose (*SI Appendix*, Table S1). Furthermore, we found no significant change in the transcript levels of the diadenylate cyclase *dacA* or c-di-AMP phosphodiesterase *gdpP* genes (relative to those for the house keeping gene *hu*, as an internal control) in response to glucose (*SI Appendix*, Table S2).

The *gdpP* gene was identified in a previous unbiased transposon screen for insertion mutants impaired in eDNA release during biofilm formation (25). The transposon screen revealed two additional genes in which mutations markedly impaired eDNA release and biofilm formation: one is *xdrA*, which encodes a transcriptional regulatory protein (37, 38). An RNAseq experiment we previously reported (25) identified transcriptional changes when *xdrA* is deleted during biofilm conditions that included genes involved in biofilm formation and virulence, but whether XdrA directly or indirectly controls these genes and how its activity is linked to c-di-AMP was not determined. The other is *apt*, which codes for an adenine phosphoribosyl transferase that generates AMP from adenine and PRPP, releasing pyrophosphate. Because Apt is involved in a purine salvage pathway, we speculated that deletion of *apt* could alter c-di-AMP levels by increasing de novo purine biosynthesis. We wondered whether *xdrA* and *apt* were also needed for the drop in c-di-AMP levels and whether this could be the basis, in whole or in part, for their involvement in biofilm formation. Accordingly, we used null mutations of each gene (Δ*xdrA* and Δ*apt*) and the riboswitch to investigate whether either or both genes were needed for the drop in c-di-AMP levels during biofilm formation. The results of Fig. 2*A* show that both mutations prevented the drop in c-di-AMP levels seen in the wild type. Indeed, the levels of the second messenger rose somewhat in both mutants, although not to the extent observed for the *gdpP* mutant. That the Δ*xdrA* and Δ*apt* mutations blocked the drop in c-di-AMP levels was independently confirmed by HPLC-mass spectrometry (*SI Appendix*, Table S1).

Next, we asked whether the effects of the mutations could be reversed by overexpression of the gene for *gdpP* using a plasmid harboring the phosphodiesterase gene (p*gdpP*). The results were particularly striking for Δ*xdrA*. The p*gdpP* plasmid increased eDNA release approximately fivefold for the Δ*xdrA* mutant (while also increasing eDNA levels for the wild type and the *gdpP* insertion mutant) (Fig. 2*B*). The plasmid also markedly increased the amount of biofilm mass of the Δ*xdrA* mutant and in a manner that was sensitive to DNase I (Fig. 2*C*). These results are consistent with the hypothesis that eDNA release and biofilm formation are caused by a drop in c-di-AMP levels and that the Δ*xdrA* mutation exerts it effect in whole or in part by blocking the drop in second messenger levels.

The results with regard to eDNA release were also striking for the Δ*apt* mutation; as seen in Fig. 2*B*, the p*gdpP* plasmid increased eDNA levels several fold in an Δ*apt* mutant. In contrast, the results with respect to biofilm formation were relatively modest; the presence of the plasmid only increased biofilm mass to a small extent (Fig. 2*C*). We note that our measurements of *gdpP* transcripts were approximately threefold elevated for Δ*apt* and Δ*apt*/Δ*xdrA* mutant strains although this is below the threshold for significance based on software guidelines (*SI Appendix*, Table S3). We conclude that like *xdrA* the *apt* gene contributes to eDNA release by lowering second messenger levels but that the Δ*apt* mutation evidently interferes with biofilm formation in some additional manner that is not bypassed by overexpressing the c-di-AMP phosphodiesterase.

Since both *xdrA* and *apt* influence the levels of c-di-AMP, we sought to determine whether they act through the same pathway by examining the levels of the second messenger in an Δ*xdrA*/Δ*apt* double mutant. The results show that the mutations exhibited an additive effect in raising c-di-AMP levels, suggesting that the genes modulate c-di-AMP levels through independent pathways (*SI Appendix*, Table S1 and Fig. 2*A*). As seen in Fig. 2*B*, the double mutant had a severe defect in eDNA release and biofilm formation. Furthermore, we found no significant change in the transcript levels of the diadenylate cyclase *dacA* or c-di-AMP phosphodiesterase *gdpP* genes in response to mutating *gdpP*::TnΩ1, Δ*xdrA,* Δ*apt, or* Δ*xdrA*/Δ*apt*, raising the possibility that DacA or GdpP is regulated at a posttranscriptional level (*SI Appendix*, Table S3).

Blocking the Drop in c-di-AMP Reduces the Ability of Cells to Form Biofilms in a Murine Model of Infection. The data so far suggests that a drop in the level of c-di-AMP is needed for *S. aureus* to form a biofilm. To investigate the biological relevance of this pathway we tested whether strains that are blocked in the drop in c-di-AMP (*gdpP*::TnΩ1, Δ*xdrA,* and Δ*apt)* are able to colonize a catheter in a murine model. In this model, we injected *S. aureus* into a subcutaneously implanted catheter and incubated it for 3 d. We then removed the catheter and surrounding tissue and measured the colony-forming units (CFU) that were associated with the catheter or were in the surrounding tissue. We found that the cell counts for the mutants *gdpP*::TnΩ1, Δ*xdrA,* and Δ*apt* were not significantly different from that for HG003 in the surrounding tissue, suggesting that blocking the drop in c-di-AMP did not have an effect on bacterial survival in the host (Fig. 3*A*). When we quantified the cells associated with that catheter, however, the numbers of cells were significantly reduced for all three mutants (Fig. 3*A*). Measurements of biofilm biomass using crystal violet

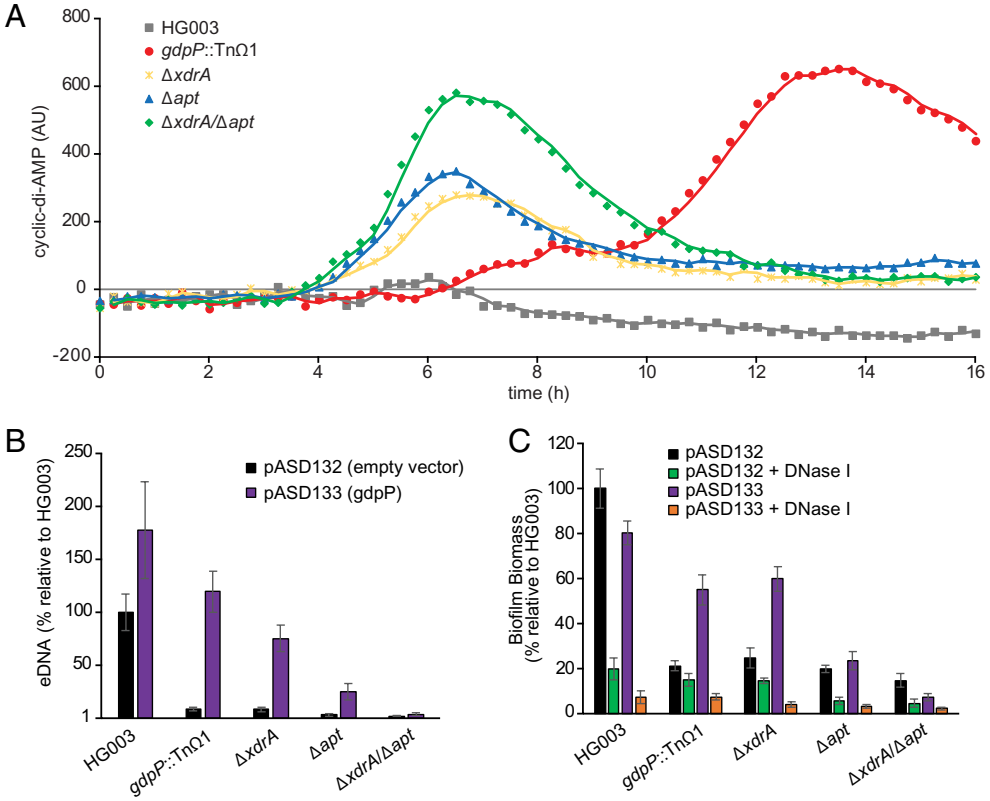

Fig. 2. Gene deletions that block reduction of cyclic-di-AMP levels prevent biofilm formation. (*A*) Cells containing a cyclic-di-AMP sensitive riboswitch biosensor were grown under biofilm promoting conditions (plus glucose). *gdpP*::TnΩ1 (red), Δ*xdrA* (yellow), Δ*apt* (blue), Δ*xdrA*/Δ*apt* (green) mutations caused elevated levels of cyclic-di-AMP compared to that of the wild-type HG003 (gray) under biofilm-forming conditions. (*B*) eDNA release and biofilm formation of the parental strains containing an empty vector plasmid (pASD132, black) or a plasmid overexpressing *gdpP* (pASD133, purple) during glucose-dependent biofilm formation. (*C*) Established biofilms were tested for sensitivity to DNase I treatment (green and orange).

staining were noisier but gave similar results whether the catheters were implanted in mice (*SI Appendix*, Fig. S2*A*) or were suspended in cultures of *S. aureus* cells (*SI Appendix*, Fig. S2*B*). Together these data demonstrate that elevated levels of c-di-AMP do not affect survival of *S. aureus* cells in the host but do affect their ability to colonize and remain associated with a catheter. Importantly, the biofilms formed on implanted catheters were sensitive to DNase (Fig. 3*B*), emphasizing that in vivo biofilms require eDNA for biofilm stability, similar to that observed for glucose-dependent biofilms formed in vitro.

c-di-AMP Controls *agr* Expression and Genes Under *agr* Control. The results so far raise the question of the nature of the downstream target of c-di-AMP that is responsible for triggering biofilm formation. A clue came from a previous RNA-seq analysis of the regulon controlled by the XdrA transcriptional regulator (25). As we have seen, an *xdrA* mutant has increased levels of c-di-AMP and hence genes in the regulon might be under the direct or indirect control of the second messenger. Noteworthy was that the most highly upregulated genes in an *xdrA* mutant under biofilm-inducing conditions compared to wildtype (HG003) cells were genes of the accessory gene regulon *agr* operon and its known downstream targets, RNAIII and the genes for the phenol soluble modulins (25, 39, 40). Together these data suggested that the increase in c-di-AMP resulting from loss of *xdrA* under biofilm conditions could cause activation of *agr*, rather than *agr* being a direct target of XdrA.

To further investigate whether elevated c-di-AMP levels cause *agr* upregulation, we determined whether a *gdpP* mutation elevates transcription of *agrA*, the gene encoding the transcriptional regulator (response regulator) of the *agr* system as well as two downstream targets, RNAIII and *psmα*. Indeed, *agrA* transcripts were four- to fivefold elevated in a *gdpP*::TnΩ1 mutant, similar to a Δ*xdrA* mutant (Fig. 4*A*). RNAIII and *psmα* transcript levels were also significantly elevated (relative to those for the house keeping gene *hu* as an internal control) (Fig. 4*A*). Conversely, artificially lowering the amount of c-di-AMP using p*gdpP* (pASD133) in wild type (HG003) cells led to a 3.5-fold decrease in *agrA* transcript levels and a significant reduction in RNAIII and *psmα* levels (Fig. 4*A*). These results suggest that *agrA* transcript levels and the downstream targets RNAIII and *psmα* are positively regulated by c-di-AMP levels.

The finding that the *agr* system is under c-di-AMP control was pleasing as previous studies had shown that the operon is repressed during biofilm formation and that mutation of the *agr* system causes a hyperbiofilm phenotype (26, 41–43). Indeed, as expected, and in our hands, an *agrA* mutation in a HG003 background caused the release of eDNA and robust biofilm formation (Fig. 4*B*). We therefore hypothesized that if elevated *agrA* transcription in a *gdpP* mutant is preventing eDNA release and biofilm formation, then Δ*agrA* should be epistatic to *gdpP*::TnΩ1. This was indeed the case as an Δ*agrA*/*gdpP*::TnΩ1 double mutant had levels of eDNA release and biofilm formation similar to those of the wild type (HG003) (Fig. 4*B*). Furthermore, using the riboswitch biosensor we found that Δ*agrA* had no effect on c-di-AMP levels (Fig. 4*C*), in keeping with the idea that *agr* is downstream of the second messenger in the pathway governing biofilm formation. Together, these results suggest that the primary mechanism by which the drop in c-di-AMP levels triggers eDNA release and biofilm formation is by lowering the level of Agr and genes under its control.

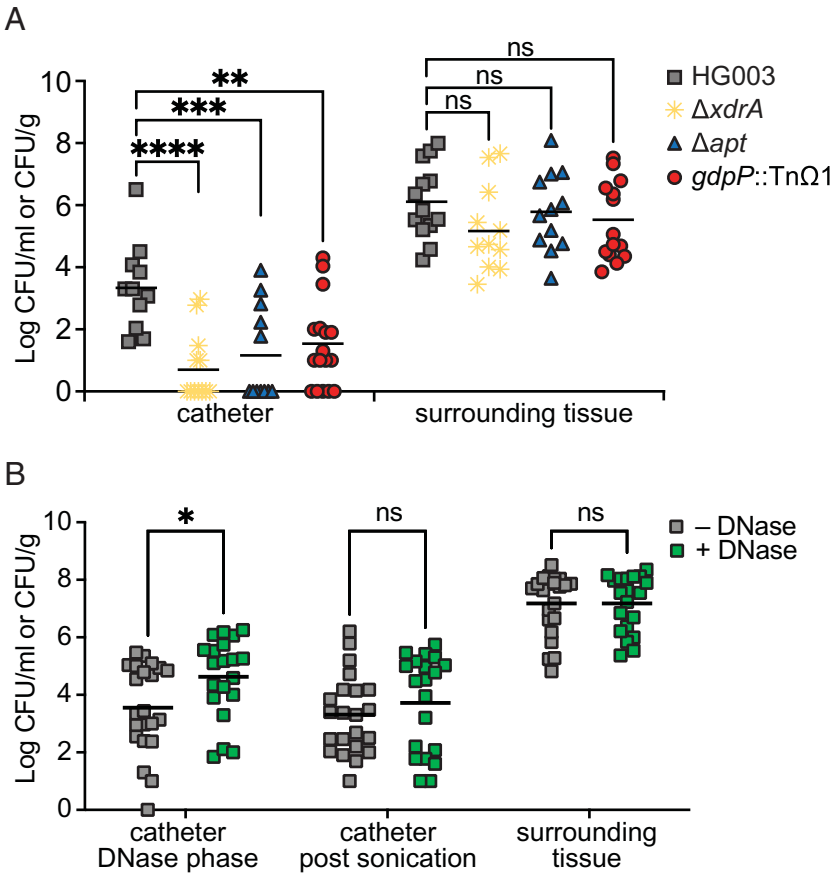

Fig. 3. c-di-AMP drop is required for biofilm formation in a murine model of infection: (*A*) Subcutaneously implanted catheters were placed in immunocompetent CFW/Swiss-webster male mice and then strains of *S. aureus* [HG003 (gray), *gdpP*::TnΩ1 (red), *ΔxdrA* (yellow), and *Δapt* (blue)] were injected into the catheter lumen. After 3 d, the catheter was removed and the colony-forming units (CFU) were measured from the catheter and surrounding tissue. Datapoints represent CFU measurements from individual animals and black lines are the mean of all measurements. Differences in bacterial load in the catheters and surrounding tissue were determined using a two-way ANOVA. (*B*) To assess the stability of catheter biofilms to DNase treatment, an initial DNase treatment phase was added to the protocol used in *A*. Subcutaneously implanted catheters in CFW/Swiss-webster male mice that were injected with the HG003 were collected 3 d after infection. The removed catheters were then placed in buffer with DNase (+ DNase, green) or without DNase (– DNase, gray) for 1 h ("DNase phase") and released CFU were measured. The catheters were then sonicated to enumerate remaining bacteria ("post sonication"). The tissue surrounding each catheter was collected and homogenized and CFU were enumerated ("surrounding tissue"). Datapoints represent CFU measurements from individual animals and black lines are the mean of all measurements. Differences were determined using a two-way ANOVA. *$P < 0.05$; **$P < 0.01$; ***$P < 0.001$; ****$P < 0.0001$; ns = not significant.

GdpP Inhibits Phosphotransfer from AgrC~P to AgrA. Our findings thus far raise the question of how c-di-AMP controls the *agr* operon. The operon, which is subject to a positive autoregulatory loop, encodes a four-protein quorum-sensing system. The pro-autoinducing peptide AgrD is processed by AgrB to cell-non-autonomously activate the histidine kinase AgrC (29, 43, 44). AgrC is autophosphorylated and then transfers the phosphate to the response regulator AgrA, which then controls transcription of downstream targets including increasing expression of the *agr* operon (43). We first considered whether c-di-AMP could directly modulate the activity of AgrC. Given that AgrC is a transmembrane protein, we reconstituted a soluble version of the Agr signaling system ($AgrC^{cyt}$) (28) for these experiments because c-di-AMP is cytoplasmic and functions cell-autonomously. Addition of millimolar c-di-AMP modestly decreased $AgrC^{cyt}$ autophosphorylation (less than 25%) and did not stimulate phospho-transfer to AgrA (Fig. 5*A*). This suggests that there is an additional factor(s) required for c-di-AMP to control Agr.

Our finding that overexpression of *gdpP* suppresses deletion of *apt* and *xdrA* led us to consider the possibility that GdpP itself could contribute to Agr regulation. Although addition of soluble GdpP ($GdpP^{cyt}$) had no effect on the autophosphorylation of $AgrC^{cyt}$ (*SI Appendix*, Fig. S2*B*), $GdpP^{cyt}$ caused a more than 2.5-fold decrease in the rate of phospho-transfer from $AgrC^{cyt}$ to AgrA (Fig. 5*B*). This is reflected both by a decrease in the rate of disappearance of phosphorylated $AgrC^{cyt}$ and by a delay in the appearance of phosphorylated AgrA (Fig. 5*B*). Supporting the specificity of this regulation, $GdpP^{cyt}$ did not change the stability of phosphorylated $AgrC^{cyt}$ in the absence of AgrA (*SI Appendix*, Fig. S2*C*) or, as a control, inhibit phospho-transfer from the *B. subtilis* histidine kinase KinA to its substrate Spo0F (Fig. 5*C* and *SI Appendix*, Fig. S2*D*). Further supporting the idea that GdpP directly inhibits AgrC phospho-transfer to AgrA, we measured submicromolar affinity binding of GdpP to full-length AgrC using microscale thermophoresis and found that GdpP reduced the affinity of AgrA binding to AgrC (Fig. 5 *D* and *E*). For MST experiments we used a further truncated form of GdpP ($GdpP^{C}$) (45) that had increased solubility and decreased noise in the binding data. Together these results demonstrate that GdpP directly inhibits Agr signaling in addition to possible effects through decreased levels c-di-AMP (Fig. 6).

While it was an attractive hypothesis that c-di-AMP acts, directly or indirectly, to control the ability of GdpP to inhibit AgrC, we detected no effect of c-di-AMP on $GdpP^{cyt}$ inhibition of $AgrC^{cyt}$ phospho-transfer (Fig. 5*B*), and c-di-AMP did not reduce the affinity of $GdpP^{C}$ for AgrC as measured by MST (Fig. 5*D*). One tantalizing result is that c-di-AMP had a small effect on reversing $GdpP^{C}$ inhibition of AgrC binding to AgrA (Fig. 5*E*). However, our inability to observe an effect of c-di-AMP in our

A

Strain	*agrA*		RNAIII		*psmα*	
Genotype	Fold change	P-Value	Fold change	P-Value	Fold change	P-Value
ΔgdpP	5	<0.005	25	<0.005	5.2	<0.005
ΔxdrA	4.1	0.02	17.4	<0.005	4.1	0.02
HG003/pASD133	-3.6	<0.005	-5.4	<0.005	-5.3	<0.005
ΔagrA	n.d.	n.d.	-17.7	<0.005	-4.2	<0.005
ΔagrA/ΔgdpP	n.d.	n.d.	-5.7	<0.005	-5.5	<0.005

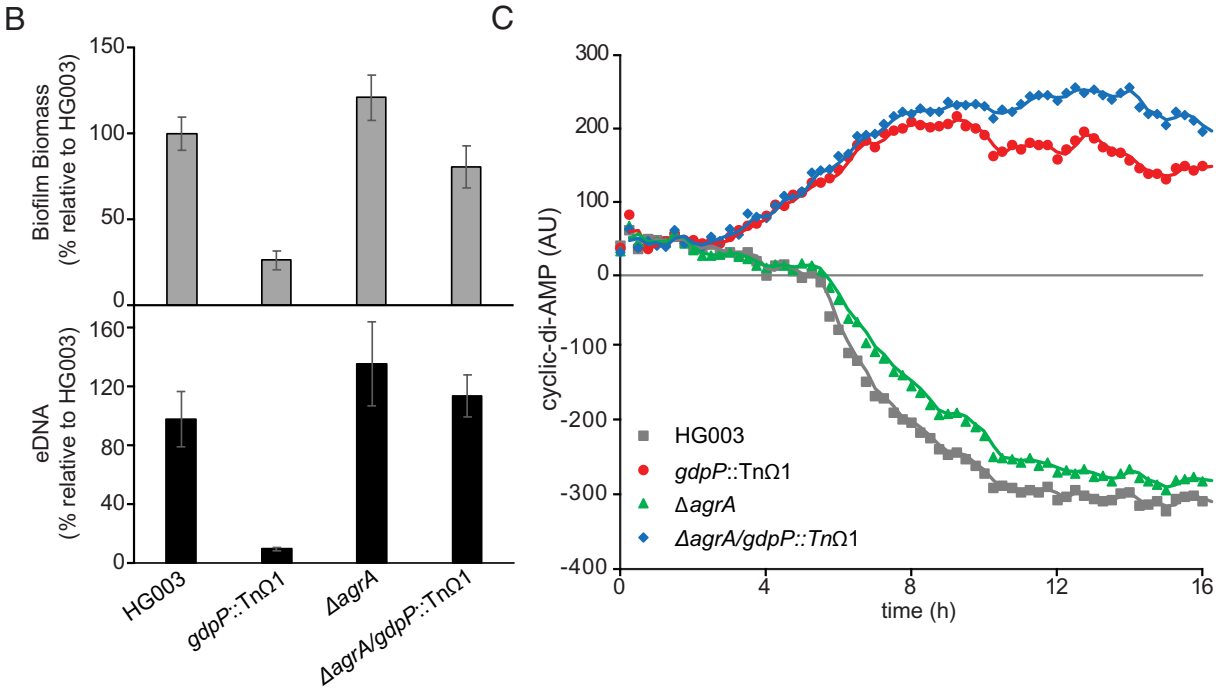

Fig. 4. An *agr* deletion mutation is epistatic to *gdpP*::TnΩ1. (*A*) Relative levels of RNA from *agrA*, RNAIII, and *psmα* are reported for *S. aureus* strains *ΔgdpP*, *ΔxdrA*, HG003 with pASD133 (*gdpP* on a plasmid), *ΔagrA*, and *ΔagrA/ΔgdpP*, grown in glucose containing medium relative to an HG003 control. Cyclic-di-AMP levels are listed as a reference based on data from Fig. 2*A*. n.d. indicates that *agrA* transcripts were not detected in *ΔagrA* cells. Unpaired two-tailed Student's *t* tests were performed, and the levels of significance are indicated. (*B*) eDNA release and biofilm formation during glucose-dependent biofilm formation. (*C*) Cells containing a cyclic-di-AMP sensitive riboswitch biosensor were grown under biofilm promoting conditions (plus glucose gray) *gdpP*::TnΩ1 (red). Mutations in Δ*agrA* (green) or Δ*agrA/gdpP*::TnΩ1 (blue) do not affect the level of cyclic-di-AMP compared to the parent strain (HG003 and *gdpP*::TnΩ1, respectively). The baseline has been normalized to HG003 no glucose.

reconstituted phospho-transfer assays (Fig. 5*B*) suggests that either this effect is insufficient to restore phosphotransfer or that the effect of c-di-AMP requires the transmembrane domain of AgrC. Thus, while these results establish a link between AgrC signaling and GdpP, they leave unanswered the question of if and how c-di-AMP acts through GdpP to control the activity of AgrC (Fig. 6).

Discussion

The principal contribution of this investigation is the finding that biofilm formation in *S. aureus* is triggered by a drop in c-di-AMP levels. Specifically, we have shown that the transition to multicellularity is accompanied by a drop in c-di-AMP levels and that this drop is prevented by null mutations of genes previously shown (and as confirmed here) to markedly impair eDNA release and biofilm formation. Further, our evidence indicates that the principal target of c-di-AMP is the *agr* system in that mutants that fail to exhibit a drop in c-di-AMP levels under biofilm-inducing conditions exhibit elevated levels of *agrA* transcripts and as well as of other genes under AgrA control (Fig. 6). Also, and importantly, an *agrA* null mutation had little effect on c-di-AMP levels but was epistatic to a *gdpP* null mutation, restoring biofilm formation in a double mutant. We therefore hypothesize that the second messenger acts through the *agr* system to control the activity of the response regulator AgrA. That is, high levels of c-di-AMP enhance expression of genes under AgrA control and low levels (under biofilm-inducing conditions) cause a drop in AgrA-directed gene expression.

Previous work has shown that c-di-AMP helps to maintain homeostasis during osmotic stress. Under conditions of increased uptake of osmolytes, the second messenger functions to maintain cell envelope integrity, in part through regulation of potassium transporter activity (and hence potassium uptake) (46–58). Thus, our present work reveals a function for c-di-AMP distinct from its role in the maintenance of homeostasis.

A major unanswered question is how the second message controls the *agr* system. A possible clue came from the surprising finding that the GdpP phosphodiesterase binds to the histidine kinase AgrC and inhibits phospho-transfer to AgrA. Our evidence indicates that this is a specific interaction in that GdpP had no measurable effect on phospho-transfer by another histidine kinase Spo0A to its substrate Spo0F. These findings suggest that GdpP is a dual function protein, acting both as a phosphodiesterase and an inhibitor of AgrC (Fig. 6).

Hence, we speculate that the second messenger acts, directly or indirectly, through GdpP, modulating its ability to block AgrC from binding to and phosphorylating AgrA. Thus, in our model low levels of c-di-AMP would allow GdpP to bind to the histidine kinase,

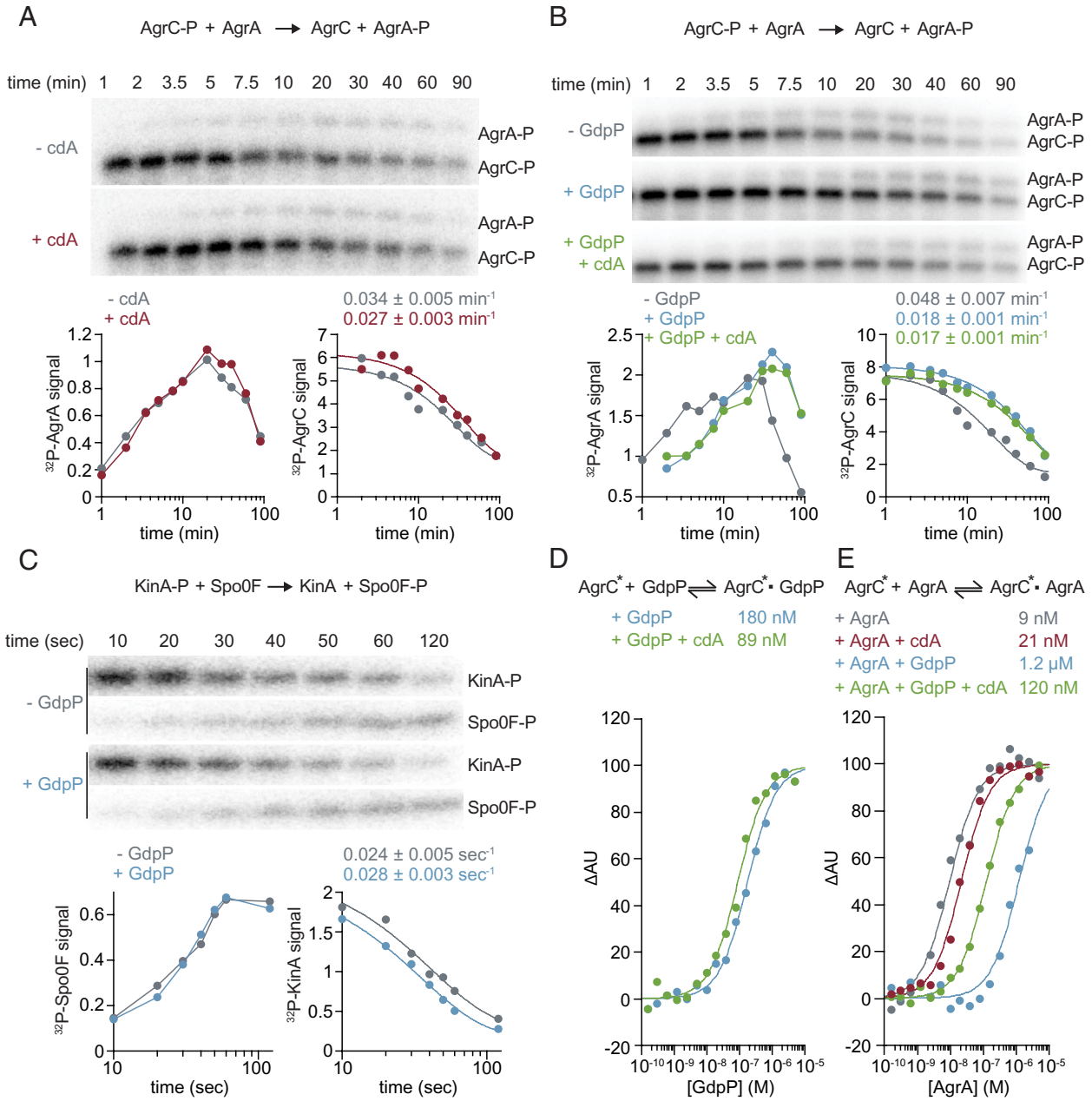

Fig. 5. GdpP inhibits AgrC phosphotransfer to AgrA. (*A* and *B*) Phosphotransfer from ^{32}P-AgrC^{cyt} (lower band, 1.25 μM) to AgrA (upper band, 10 μM) is shown in the absence (*Top*) and presence (*Bottom*) of cyclic-di-AMP (1 mM) (*A*) or GdpP^{cyt} (20 μM) as indicated by the reaction scheme. Radioactive gels were imaged by phosphorimaging and band intensities were quantified below for ^{32}P-AgrA signal (*Left*, which accumulates and then disappears due to spontaneous hydrolysis) and ^{32}P-AgrC^{cyt} signal (*Right*). Data for AgrC^{cyt} signal were fit to an exponential decay function with rates indicated on the plots. (*C*) Phosphotransfer from ^{32}P-KinA from *B. subtilis* (upper images, 0.1 μM) to Spo0F (lower images, 0.2 μM) is shown in the absence (*Top*) and presence (*Bottom*) of GdpP^{cyt} (20 μM). KinA (69 kDa) and Spo0F (14 kDa) bands are shown cropped from the same gels. Plots show quantification as in (*A*) and (*B*). (*D*) MST dose–response curve (change in absorbance plotted against ligand concentration) for labeled AgrC incubated with serially diluted GdpP^{C} (*Left*) in the presence (green) and absence (blue) of 100 μM cyclic-di-AMP. Data were fit to a binding model and dissociation constants are labeled above graphs. (*E*) MST dose–response curve for labeled AgrC incubated with serially diluted AgrA (*Right*) in the presence (red) and absence (gray) of 100 μM cyclic-di-AMP, presence (blue) of 200 nM GdpP^{C}, and presence (green) of 100 μM cyclic-di-AMP and 200 nM GdpP^{C}. The reaction scheme is diagrammed above the plots. Data are plotted with a logarithmic X-axis. Data were fit to a binding model and dissociation constants are labeled above graphs. Reported errors are the errors of the fits and all plots have a logarithmic X-axis.

thereby inhibiting the activation of the response regulator AgrA and triggering biofilm formation. In contrast, high levels of the cyclic dinucleotide would interfere with GdpP's inhibition of AgrC binding to AgrA, thereby allowing activation of the *agr* system, which impedes biofilm formation (26, 41–43). It remains to be determined, however, if and how c-di-AMP acts to influence the interaction of GdpP with AgrC, if indeed our hypothesis is correct. This could be mediated by a direct interaction of c-di-AMP with GdpP, although efforts to detect a reversal of GdpP-mediated inhibition by c-di-AMP (or its hydrolysis product pApA) have been unsuccessful. Alternatively, the c-di-AMP pathway controlling AgrC activity could require another as yet unidentified partner (Fig. 6).

We note that transcription of the *agr* system is subject to quorum sensing via the Autoinducing Peptide (43). Thus, high levels of the autoinducer set up a positive feedback loop in which AgrA stimulates transcription of genes in the *agr* system (59). We posit that this positive feedback loop renders expression of the *agr* system hypersensitive to GdpP. Thus, when c-di-AMP levels are low, inhibition of AgrC by GdpP would prevent the self-reinforcing cycle of *agr* expression whereas low level of the cyclic dinucleotide

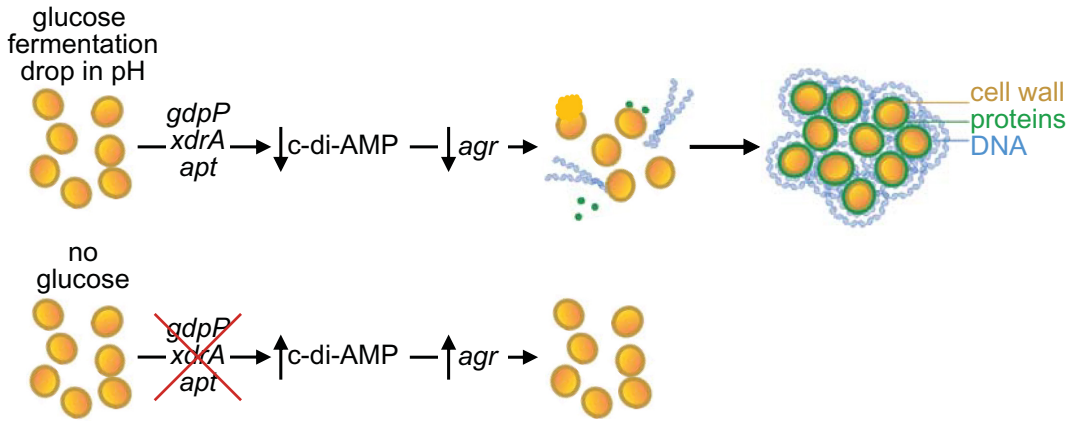

Fig. 6. Model for the role of GdpP in biofilm formation. A schematic is shown summarizing how GdpP controls biofilm formation. *gdpP*, *xdrA,* and *apt* together are required for a biofilm-associated drop in the levels of c-di-AMP. This drop in c-di-AMP is in turn required for biofilm formation through inhibition of Agr. In media lacking glucose or when *gdpP*, *xdrA*, or *apt* are deleted, c-di-AMP levels remain high, preventing inhibition of Agr and biofilm formation.

would limit expression of the *agr* system and hence AgrA-directed gene expression.

Another important unanswered question is how AgrA negatively controls biofilm formation (26, 41–43). A well-known target of AgrA is RNAIII, and indeed, the *gdpP* mutation markedly stimulated RNAIII transcript levels (Fig. 4*A*). However, the known targets of RNAIII do not provide any obvious clues as to how they might control biofilm formation (e.g., genes needed for cell envelope integrity that might lead to cell lysis when their expression is impaired). The *agr* operon also controls transcription of genes for a class of small proteins known as the phenol soluble modulins (PSMs). And indeed these modulins are reported to promote biofilm dispersal (60). However, their role in dispersal does not suggest a mechanism for how they could block biofilm formation and eDNA release. The PSM's have also been reported to form amyloid-like fibers that stabilize *S. aureus* biofilms, but these fibers have not been detected in glucose-dependent biofilms (61). Finally, it is not known how other changes associated with biofilm formation such as production of adhesins and clumping factors might be correlated with c-di-AMP levels and GdpP activity. In toto, our results suggest that an as yet unidentified target(s) of *agr* is responsible for impeding biofilm formation under conditions of high levels of c-di-AMP.

Finally, also unanswered is the question how the drop in c-di-AMP levels is brought about under biofilm-inducing conditions. We found no significant difference in transcript levels of *dacA* or *gdpP* in response to glucose, suggesting that regulation of c-di-AMP occurs at a posttranscriptional level (*SI Appendix*, Table S3). Our finding that *xdrA* and *apt* are upstream of the drop in c-di-AMP and inhibition of Agr suggest that these genes are involved in initiating the switch to biofilm formation. How the activity of these genes is controlled and how they control downstream pathways to dictate c-di-AMP levels are important unanswered questions. Previous studies have shown that the degradation product of c-di-AMP, 5′-phosphonoadenylyl-adenosine (pApA), as well as the alarmone (p)ppGpp are able to inhibit GdpP (62, 63), raising the possibility that the drop in c-di-AMP levels during biofilm formation is mediated at the level of the activity of GdpP. Intriguingly, *apt* and alterations in intracellular purine nucleotide levels have been shown to control levels of (p)ppGpp and c-di-AMP (64, 65), suggesting a possible mechanistic link.

Biofilm formation by *S. aureus* is critical to the formation of recalcitrant infections, such as infective endocarditis and postsurgical infections on indwelling medical devices (15, 18, 66–68). Once biofilms become established, they are resistant to antimicrobial treatments, making the infection difficult to eradicate. This antimicrobial resistance is complicated by the emergence of antibiotic resistant strains of *S. aureus* (MRSA and VRSA) (69). Attempts have been made to prevent *S. aureus* biofilm infections by activating AgrC. These studies are based on the premise that activating the *agr* system would prevent biofilm formation or cause the biofilms to disperse. However, molecules stimulating AgrC have so far proved ineffective in treating a *S. aureus* biofilm infection (70). Our work offers a possible explanation for the failure of such compounds: under low c-di-AMP conditions, inhibition of AgrC by GdpP could be preventing AgrC from activating AgrA even in the presence of AgrC-stimulating agents.

Instead, our finding that loss of GdpP function blocks *S. aureus* biofilm formation suggests that GdpP may be an attractive target for biofilm-blocking drugs. Importantly, many phosphodiesterase inhibitors have been developed to treat multiple conditions in humans (71–73). Although these phosphodiesterases are structurally distinct from GdpP, the ability to create safe and effective drugs that target these enzymes brings merit to the idea of obtaining an inhibitor of a bacterial phosphodiesterase.

Materials and Methods

Strains and Growth Conditions. The *S. aureus* strains used in this study are listed in *SI Appendix*, Table S4 and *E. coli* strains are listed in *SI Appendix*, Table S5. *S. aureus* were maintained in Tryptic Soy Broth (TSB) with no glucose [17 g/L of Peptone for Casein (BD); 3 g/L of Peptone from Soymeal (Amresco); 5 g/L of NaCl (Sigma); 2.5 g/L of dipotassium hydrogen phosphate (Macron)] or TSB with 0.5% glucose (TSBg). Unless noted, all experiments were performed in TSBg. Selection for drug resistance was maintained using 10 μm/mL Chloramphenicol for *S. aureus*. *gdpP*::TNΩ1 strains were made by transduction via Φ85. Plasmids were incorporated using electroporation. Riboswitch (pCDAribo) was synthesized by Integrated DNA Technologies (IDT; Coralville, Iowa) and moved into pASD132 using restriction cloning. The sequence of the riboswitch is (36): AGCTTAGATC TCGATCCCGCGAAATTAATACGACTCACTATAGGGGCCCGGATAGCTCAGTCGGTAGAGC AGCGGCCGGATGTAACTGAATGAAATGGTGAAGGACGGGTCCAGCTTAATCAAACAC GAACGGGGGAACCAACGATTGGCTGTTTTATTAACAGCCTTGGGGTGAATCTTACTAAGT AAGAGGGGGTACTCTGAATCCCTAATCCGACAGCTAACCTCGTAGGCTTGTTGAGTAGAGTGT GAGCTCCGTAACTAGTTACATCCGGCCGCGGGTCCAGGGTTCAAGTCCCTGTTCGGGCGCC ATAGCATAACCCCTTGGGGCCTCTAAACGGGTCTTGAGGGGTTTTTTGCTCGAG.

Biofilm Assay. *S. aureus* overnight cultures were diluted 1:200 into 200 μL of fresh TSB or TSBg per well of a Nunc MicroWell 96-well plate (no. 167008; ThermoFisher) and incubated statically at 37 °C for 24 h. When specified 10 U of DNase I (04716728001; Roche) were added to the biofilms after 23 h and were

then returned to 37 °C for one additional hour. The medium was then carefully removed and the biofilms were washed three times with 200 μL of PBS at pH 7.5. 100 μL of 0.1% Crystal Violet stain was then added to each well for 5 min. The Crystal Violet was then carefully removed and the biofilms were gently washed three times with 200 μL of PBS at pH 7.5. The stained biofilms were then dried at room temperature. Once dry, 200 μL of acidified ethanol was added to each well. 50 μL of the resuspended stained cells was then transferred to a fresh microtiter plate with 150 μL of PBD at pH 7.5 and the OD600 was immediately measured using a plate reader (Infinite 200 Pro, Tecan). The background value of stained wells without any inoculum was subtracted from the readings and averages and SD were calculated. Biofilm biomass was calculated to be relative to the WT HG003 biofilm.

eDNA Measurements. Biofilms were grown as described above. Once the biofilms were grown for 24 h they were washed three times with 200 μL of PBS at pH 7.5 and then resuspended in 200 μL of PBS at pH 7.5 and transferred to a filter plate (90.2 μm AcroPrep Advance 96-well filter plates No. 8019; Pall). 100 μL of the filtrate was then combined with 100 μL of 2 μM SYTOX Green (No. S7020; ThermoFisher) in PBS. Fluorescence was then measured using a plate reader (Infinite 200 Pro, Tecan) with excitation and emission wavelengths of 465 nm and 510 nm, respectively. The values from uninoculated wells were subtracted from the readings and averages and SD were calculated. The amount of eDNA present was calculated to be relative to that of the WT HG003 biofilm.

Visualizing Cell Clumping. Biofilms were grown as described as above. After 24 h of growth, cells were gently resuspended using one gentle aspiration and dispensation of the medium they were grown in. 1 μL of each sample was then placed on an agar pad and visualized using a Nikon Eclipse Ti inverted microscope equipped with an Orca R2 (Hamamatsu) camera and a 10×/0.30 Plan Fluor air objective (Nikon).

Riboswitch Assay. *S. aureus* strains containing pASD132 (empty vector) or pASD containing a cyclic-di-AMP riboswitch (pCDAribo) were grown in TSB or TSBg with 20 μg/mL of chloramphenicol, 0.01% Trypan Blue (Invitrogen), and 250 μM of DFHBI-1T (No. 5610; Tocris) overnight shaking at 37 °C in a plate reader (Tecan Infinite 200 Pro or Bio Tek Cytation5) with excitation and emission wavelengths of 460 nm and 510 nm, respectively, for 16 h. At each time point the empty vector fluorescence was subtracted from the pCDAribo strains to remove autofluorescence. Excluding Fig. 1*A* the baseline for the assays was normalized to HG003 grown with no added glucose. Values are reported as arbitrary units (AU).

qPCR. *S. aureus* overnight cultures were diluted 1:200 into 3 mL of fresh TSB or TSBg per well of a Nunc MicroWell 6-well plate (No. 140675; ThermoFisher) and incubated statically at 37 °C for 6 h. 6 mL of RNA Protect Bacterial Reagent was added to each sample and biofilms were immediately resuspended by pipetting. The cells were pelleted at 5k × g for 5 min and resuspended in 1 mL Trizol. Cells were then mechanically disrupted using a FastPrep-24 (MP Biomedicals). Chloroform extraction of Trizol was done to isolate RNA. RNA was incubated with 10 U of DNase I (Roche) for 90 min at 37 °C to remove any DNA contamination followed by phenol/chloroform extraction to purify the RNA. cDNA was made using the Superscript IV first-strand synthesis system (18091050, ThermoFisher). qPCR was performed using QuantiTect SYBR Green (204145, Qiagen) and run on a BioRad CFX384. Data were analyzed using BioRad CFX analyzer 3.1. Data were normalized to transcript levels of the reference gene SAOUHSC_01490 (*hu*). Primers were designed using Geneious 11.0.5. Primers for qPCR are listed in *SI Appendix*, Table S6.

Murine Model of *S. aureus* Catheter-Associated Biofilm Infection. Immunocompetent CFW/Swiss-webster male mice (5 to 7 wk) were used (Charles River Laboratory, Wilmington, MA). Mice were housed in an individually ventilated cage system under specific-pathogen-free conditions, and water and food were supplied ad libitum. Experiments were approved by the Institutional Animal Care and Use Committee (IACUC) at Massachusetts General Hospital.

Mice were anesthetized in an anesthesia chamber prefilled with 1.5% isoflurane (Patterson Veterinary, St. Paul, MN) in oxygen for 15 min. Then, the hair from the flank region was removed, and the surgical field was sterilized. A 1-cm subcutaneous incision was made in the flank using a sterile blade and a blunt probe was used to create a subcutaneous pocket for advancing a 1-cm sterile Teflon-coated catheter (Exel International, St. Petersburg, FL). The skin incision was sealed with Vetbond tissue adhesive (3M, St. Paul, MN). A total of 10^3 CFU of *S. aureus* in 20 μL of PBS was injected directly into the catheter lumen to establish biofilm formation. Animals were monitored daily thereafter. On day 3 postinfection, animals were killed with an overdose of CO_2. The skin was disinfected, and catheters were removed, washed with 500 μL of PBS to remove the loosely attached planktonic bacteria, and placed in a tube containing 1 mL of PBS. Catheters were sonicated for 3 min (pulse 30 s on, 30 s off with 10% amplitude), vortexed, and plated to enumerate the CFU/ml of biofilm-associated bacteria. The tissue around the catheter was taken, placed in 1 mL of PBS, homogenized, and plated to enumerate the CFU/g. Data are presented as means ± SEM. Differences in bacterial load in the catheters and surrounding tissue were determined using a two-way ANOVA (GraphPad Prism 9.3.1). A P value < 0.05 was considered significant.

Additionally, a DNAse treatment protocol was implemented to assess the importance of eDNA to biofilm stability. Following the previously described infection protocol, mice were infected, and on day 3, catheters were surgically removed. To assess DNase sensitivity of the biofilm (DNase phase), each catheter was washed with 500 μL of PBS and then placed in a microcentrifuge tube containing 1 mL of PBS with or without 10 μL of DNAse (Roche, 10 U/μL). All samples (whether DNase was added or not) were incubated at 37 °C for 1 h, and plated to enumerate CFU/mL. Subsequently, the same catheters were subjected to a second wash with 500 μL of PBS and transferred to a 15 mL tube containing an additional 1 mL of PBS. The catheters were then sonicated for 3 min using a pulsing method (30 s on, 30 s off at 10% amplitude), vortexed, and plated to enumerate CFU/mL of bacteria that remained adhered to the catheter after DNase treatment. Finally, for each mouse, the tissue around the catheter was taken, placed in 1 mL of PBS, homogenized, and plated to enumerate the CFU/g.

Crystal Violet In Vitro and In Vivo. To study bacterial biofilm formation in vitro, overnight cultures in TSB with and without 0.5% glucose were diluted to 5×10^5 CFU/mL. Five milliliters of each culture were transferred into tubes containing either 0.5% glucose or no glucose, with a catheter placed in each tube. After 3 d of incubation at 37 °C, catheters were removed, washed with 1 mL of PBS, and placed in a 24-well plate for biofilm analysis using a crystal violet assay. Catheters were washed twice with 1 mL of water, stained with 1 mL of 0.1% crystal violet for 30 min, then washed three times with water and fixed with 30% acetic acid. After 30 min, the OD at 595 nm was measured. For in vivo biofilm assessment, catheters were removed, washed with 500 μL of PBS, and subjected to the same crystal violet assay protocol as described for in vitro analysis.

Data are presented as means ± SEM. Differences in in vitro biofilm biomass were determined using a two-way ANOVA. Differences in in vivo biofilm biomass were determined using the Kruskal–Wallis test with Dunn post hoc testing (GraphPad Prism 9.3.1). A P value < 0.05 was considered significant.

Protein Expression and Purification. All proteins were expressed in *E. coli* BL21 (DE3) cells grown at 37 °C to an OD_{600} of 0.4 and induced at 16 °C for 14 to 18 h with 1 mM isopropyl β-d-1-thiogalactopyranoside (IPTG) unless otherwise specified. Cells were harvested and purified as follows:

AgrC*^{cyt} *(222–430). AgrC^{cyt} expression cells were grown at 37 °C to an OD_{600} of 0.4 and induced at 37 °C for 4 h. Cell pellets were resuspended in lysis buffer with 1 mM phenylmethylsulfonyl fluoride (PMSF) (30 mM Na_2HPO_4, 5 mM NaH_2PO_4, pH 7.4, 500 mM NaCl), and were lysed using two passes in a microfluidizer at 10,000 PSI. Cell lysates were cleared by centrifugation for 45 min at 16,000 RPM. Cell lysates were then run over a HisTrap HP column on an AKTA FPLC, washed with lysis buffer with 40 mM imidazole, and eluted with a gradient to 500 mM imidazole. Fractions were pooled and further purified on a Superdex200 16/600 column equilibrated with 50 mM Tris·HCl, 15 mM K·HEPES pH 7.8, 100 mM NaCl, 10 mM $MgCl_2$, 1 mM tris -(2-carboxyethyl) phosphine (TCEP) on an AKTA FPLC. Fractions were pooled, concentrated to 200 μM, flash-frozen, and stored at −80 °C.

AgrA. Cell pellets were resuspended in lysis buffer with 1 mM PMSF (20 mM Tris·HCl, pH 8.0, 100 mM NaCl, 20% glycerol, 1 mM TCEP) and were lysed using two passes in a microfluidizer at 10,000 PSI. Cell lysates were cleared by centrifugation for 45 min at 16,000 RPM. Cell lysates were then batch bound with 4 mL of pre-equilibrated Ni-NTA resin/L of cells for 1 h. Resin was then flowed over a gravity column and washed with 5 column volumes of wash 1 buffer (20 mM Tris·HCl, pH 8.0, 500 mM NaCl, 15 mM imidazole, 20% glycerol, 1 mM TCEP) and 10 column volumes of wash 2 buffer (20 mM Tris·HCl, pH 8.0, 100 mM NaCl, 35 mM imidazole, 20 % glycerol, 1 mM TCEP). AgrA was eluted in 1.5 CV of elution buffer (20 mM Tris·HCl, pH 8.0, 100 mM NaCl, 300 mM imidazole, 20% glycerol,

1 mM TCEP). AgrA was then concentrated to 2.5 mL with sucrose and run on a Superdex75 16/60 column equilibrated in lysis buffer on an AKTA FPLC. Fractions were collected, concentrated with sucrose to 20 μM, buffer exchanged into assay buffer with 20% glycerol (50 mM Tris·HCl, pH 7.2, 100 mM KCl, 5 mM $MgCl_2$, 20% glycerol) flash-frozen, and stored at −80 °C.

GdpP^{cyt} (86–655). Cell pellets were resuspended in lysis buffer with 1 mM PMSF (25 mM Tris·HCl, pH 8.0, 300 mM NaCl) and were lysed using two passes in a microfluidizer at 10,000 PSI. Cell lysates were cleared by centrifugation for 45 min at 16,000 RPM. Cell lysates were then run over 4 mL of pre-equilibrated Ni-NTA resin/L of cells on a gravity column. Resin was then washed with 10 column volumes of lysis buffer with 20 mM imidazole. GdpP was eluted with lysis buffer with 300 mM imidazole. GdpP was then concentrated and run on a Superdex200 16/600 column equilibrated in 10 mM Tris·HCl, pH 8.0, and 300 mM NaCl on an AKTA FPLC. Fractions were pooled, concentrated to 30 μM, flash-frozen, and stored at −80 °C.

KinA. KinA expression cells were grown at 37 °C to an OD_{600} of 0.4 and induced at 30 °C for 6 h. Cell pellets were resuspended in lysis buffer with 1 mM PMSF and 1 mg/mL lysozyme (20 mM Tris·HCl, pH 8.0, 150 mM NaCl) and were lysed using two passes in a microfluidizer at 10,000 PSI. Cell lysates were cleared by centrifugation for 45 min at 16,000 RPM. Cell lysates were then run over a HisTrap HP column pre-equilibrated with lysis buffer with 20 mM imidazole on an AKTA FPLC, washed with lysis buffer with 30 mM imidazole, and eluted with a gradient to 200 mM imidazole. KinA was further purified on a Superdex200 16/600 equilibrated with 25 mM bis-Tris pH 7.2, 50 mM KCl, 0.1 mM EDTA. 10% glycerol. Fractions were pooled, concentrated to 100 μM, flash-frozen, and stored at −80 °C.

Spo0F. Spo0F expression cells were grown at 37 °C to an OD_{600} of 0.4 and induced at 30 °C for 6 h. Cell pellets were resuspended in lysis buffer with 1 mM PMSF (20 mM Tris·HCl, pH 7.9, 500 mM NaCl, 5 mM imidazole, 0.1% Triton X100) and were lysed using two passes in a microfluidizer at 10,000 PSI. Cell lysates were cleared by centrifugation for 45 min at 16,000 RPM. Cell lysates were batch bound with 4 mL of pre-equilibrated Ni-NTA resin/L of cells in lysis buffer for 1 h. Resin was then flowed over a gravity column and washed with 10 column volumes of wash buffer (20 mM Tris·HCl, pH 7.9, 500 mM NaCl, 15 mM imidazole). Spo0F was eluted with elution buffer (20 mM Tris·HCl, pH 7.9, 500 mM NaCl, 50 mM imidazole). Spo0F was further purified on a Superdex75 16/60 equilibrated with 25 mM bis-Tris pH 7.2, 50 mM KCl, 0.1 mM EDTA. 10% glycerol. Fractions were pooled, concentrated to 100 μM, flash-frozen, and stored at −80 °C.

Full-length AgrC. Cell pellets were resuspended in lysis buffer with 1 mM PMSF, 1 mg/mL lysozyme, and DNaseI (20 mM Tris·HCl, pH 8.0, 100 mM NaCl, 1 mM TCEP) and lysed. Cell lysate was centrifuged at 15,000×*g* for 10 min, then the supernatant was ultracentrifuged in a 45 Ti for 1 h at 37,000 RPM. The supernatant was then discarded and the pellet was resuspended in a glycerol buffer with 0.5 mM PMSF (20 mM Tris·HCl, pH 8.0, 100 mM NaCl, 20% v/v glycerol). The homogenized pellet was then flash-frozen and stored at −80 °C.

The homogenized pellet thawed in ice-water bath for 45 min. Membranes were stirred on ice for 3 h with 0.5 mM PMSF and 2% n-dodecyl-β-D-maltoside (DDM). Membranes were ultracentrifuged for 30 min at 37,000 RPM. The supernatant was filtered through a 0.45 μM Durapore PVDF filter and batch bound with 4 mL of pre-equilibrated Ni-NTA resin in 20 mM Tris·HCl, pH 8.0, 100 mM NaCl, 1 mM TCEP for 1 h. Resin was flowed over gravity column and washed with 5 column volumes of high salt soapy buffer (20 mM Tris·HCl, pH 8.0, 500 mM NaCl, 15 mM imidazole 1 mM TCEP, 0.05% DDM) and 10 column volumes of low salt soapy buffer (20 mM Tris·HCl, pH 8.0, 100 mM NaCl, 25 mM imidazole 1 mM TCEP, 0.05% DDM). Full-length AgrC was eluted with 3 column volumes of elution buffer (20 mM Tris·HCl, pH 8.0, 100 mM NaCl, 200 mM imidazole 1 mM TCEP, 0.05% DDM). Full-length AgrC was then concentrated and purified further on a Superdex200 16/600 column equilibrated in 20 mM Tris·HCl, pH 8.0, 100 mM NaCl, 1 mM TCEP, 0.05% DDM. Fractions were pooled, concentrated to 50 μM, flash-frozen, and stored at −80 °C.

GdpP^{C} (315–655). GdpP^{C} expression cells were grown at 37 °C with 0.5 M $MnCl_2$ to an OD_{600} of 0.6 and induced at 18 °C for 14 to 18 h. Cell pellets were resuspended in lysis buffer with 1 mM PMSF and 1 mg/mL lysozyme (20 mM Tris·HCl, pH 8.0, 300 mM NaCl). Cells were lysed with a sonicator. Lysate was spun at 4,200 RPM for 10 min and then ultracentrifuged at 37,000×*g* for 1 h. Cell lysates were then batch bound to 5 mL of pre-equilibrated resin in lysis buffer with 20 mM imidazole for 1 h. Resin was flowed over gravity column and washed with 3 column volumes of lysis buffer with 20 mM imidazole. GdpP^{C} was eluted in elution buffer (20 mM Tris·HCl, pH 8.0, 300 mM NaCl, 200 mM imidazole), concentrated to 30 μM, flash-frozen, and stored at −80 °C.

Phosphotransfer Assays. AgrC^{cyt} was labeled with ^{32}P by incubating AgrC^{cyt} (100 μM) with 10 μCi of γ-^{32}ATP for 2 h at room temperature in 50 mM Tris·HCl, 15 mM K·HEPES, pH 7.8, 100 mM NaCl, 10 mM $MgCl_2$, 1 mM TCEP. Unincorporated nucleotide was removed by buffer exchange using a Zeba spin column equilibrated in 50 mM Tris·HCl, pH 7.2, 100 mM KCl, 5 mM $MgCl_2$.

KinA was labeled with ^{32}P by incubating KinA (100 μM) with 10 μCi of γ-^{32}ATP for 2 h at room temperature in 50 mM Tris·HCl, pH 8.5, 20 mM $MgCl_2$, 10 mM KCl, 5% glycerol. Unincorporated nucleotide was removed by buffer exchange using a Zeba spin column equilibrated in 50 mM Tris·HCl, pH 8.5, 20 mM $MgCl_2$, 10 mM KCl, 5% glycerol.

All phosphotransfer assays were performed at room temperature. AgrC^{cyt} phosphotransfer assays were performed in 50 mM Tris·HCl, pH 7.2, 100 mM KCl, 5 mM $MgCl_2$. The concentrations of enzyme and substrate were varied as indicated. 100 μM or 1 mM of cyclic-di-AMP was additionally added to reactions as indicated. Reactions were stopped with SDS loading buffer, then run on a 12% Tris-Glycine BioRad gel. The gel was then fixed for 1 h in 40% isopropanol and phosphorimaged on a Typhoon scanner. KinA phosphotransfer assays were performed similarly except that the reaction buffer was 50 mM Tris·HCl, pH 8.5, 20 mM $MgCl_2$, 10 mM KCl, 5% glycerol, and gels were not fixed prior to imaging. Assays were performed more than three independent times as separate experiments. Data shown in figures are from a single representative experiment, and reported errors are the errors from the fit.

MicroScale Thermophoresis (MST). A NanoTemper Monolith NT.115 was used for MST experiments and all Monolith products used are from NanoTemper Technologies GmbH. After FPLC purification and concentration in buffer (20 mM Tris·HCl, pH 8.0, 100 mM NaCl, 5 mM TCEP, 0.05% DDM), full-length AgrC was labeled with Monolith NT-647-Red dye (Cat# MO-L018) using the manufacturer's labeling protocol. Labeled full-length AgrC was split into 16 aliquots and mixed to a final concentration of 10 nM with GdpP or AgrA for 5 min (the optimal range of ligand concentration was determined experimentally after a binding curve was established, but always consisted of 16 concentrations of ligand across a twofold serial dilution). GdpP used for MST was the GdpP-C construct that lacks the PAS domain, and AgrA used for MST was the AgrA annotated from the NCTC8532 strain of *S. aureus*. Samples were transferred to Monolith NT.115 Capillaries (Cat# MO-K022) and loaded onto the instrument. MO. Affinity Analysis software was used for dataset processing and analysis.

Arbitrary fluorescence values for each sample were generated from average fluorescence on the MST curve between 0.5 s and 1.5 s after the initiation of thermophoresis, normalized by comparison with average fluorescence from 1 s and 0 s prior to thermophoresis. These were plotted against ligand concentration to generate a binding curve. Data were fitted to the K_D model and CI of the K_D was calculated from the variance of the fitted curve.

Data, Materials, and Software Availability. All study data are included in the article and/or *SI Appendix*.

ACKNOWLEDGMENTS. Funding for this work was provided by NIH Grant PO1-AI083214 to R.L. and D.K., NIH Grant R01 AI057576 to D.C.H., Startup funds from Brandeis University to N.B., and a Real Colegio Complutense Fellowship to M.L.G.-M. We thank former undergraduates Eliza Llewellyn and Claudio Reck Rivera for participating in this work. We thank Angelika Gründling and Alexander Horswill for helpful comments on the manuscript.

Author affiliations: [a]Department of Molecular and Cellular Biology, Harvard University, Cambridge, MA 02138; [b]Department of Biochemistry, Brandeis University, Waltham, MA 02453; [c]Department of Chemistry and Chemical Biology, Harvard University, Cambridge, MA 02138; and [d]Division of Infectious Disease, Massachusetts General Hospital, Boston, MA 02114

Author contributions: A.K.S., R.B., E.R.V.V., M.L.G.-M., D.C.H., D.K., R.L., and N.B. designed research; A.K.S., R.B., E.R.V.V., M.L.G.-M., and T.L. performed research; A.K.S., R.B., E.R.V.V., M.L.G.-M., T.L., D.C.H., D.K., R.L., and N.B. analyzed data; and A.K.S., R.B., E.R.V.V., M.L.G.-M., D.C.H., D.K., R.L., and N.B. wrote the paper.

1. K. Schilcher, A. R. Horswill, Staphylococcal biofilm development: Structure, regulation, and treatment strategies. *Microbiol. Mol. Biol. Rev.* **84**, e00026-19 (2020), 10.1128/MMBR.00026-19.
2. V. Dengler, L. Foulston, A. S. DeFrancesco, R. Losick, An electrostatic net model for the role of extracellular DNA in biofilm formation by *Staphylococcus aureus*. *J. Bacteriol.* **197**, 3779–3787 (2015).
3. E. E. Mann *et al.*, Modulation of eDNA release and degradation affects *Staphylococcus aureus* biofilm maturation. *PLoS ONE* **4**, e5822 (2009).
4. E. S. Gloag *et al.*, Self-organization of bacterial biofilms is facilitated by extracellular DNA. *Proc. Natl. Acad. Sci. U.S.A.* **110**, 11541–11546 (2013).
5. L. Turnbull *et al.*, Explosive cell lysis as a mechanism for the biogenesis of bacterial membrane vesicles and biofilms. *Nat. Commun.* **7**, 375 (2016).
6. C. B. Whitchurch, T. Tolker-Nielsen, P. C. Ragas, J. S. Mattick, Extracellular DNA required for bacterial biofilm formation. *Science* **295**, 1487 (2002).
7. S. S. Branda, Å. Vik, L. Friedman, R. Kolter, Biofilms: The matrix revisited. *Trends Microbiol.* **13**, 20–26 (2005).
8. S. S. Branda, F. Chu, D. B. Kearns, R. Losick, R. Kolter, A major protein component of the *Bacillus subtilis* biofilm matrix. *Mol. Microbiol.* **59**, 1229–1238 (2006).
9. D. O. Serra, A. M. Richter, R. Hengge, Cellulose as an architectural element in spatially structured *Escherichia coli* biofilms. *J. Bacteriol.* **195**, 5540–5554 (2013).
10. M. R. Chapman *et al.*, Role of *Escherichia coli* curli operons in directing amyloid fiber formation. *Science* **295**, 851–855 (2002).
11. L. Foulston, A. K. W. Elsholz, A. S. DeFrancesco, R. Losick, The extracellular matrix of *Staphylococcus aureus* biofilms comprises cytoplasmic proteins that associate with the cell surface in response to decreasing pH. *mBio* **5**, e01667-14 (2014).
12. M. L. Hanke, T. Kielian, Deciphering mechanisms of Staphylococcal biofilm evasion of host immunity. *Front. Cell. Infect. Microbiol.* **2**, 62 (2012), 10.3389/fcimb.2012.00062.
13. M. Bhattacharya *et al.*, *Staphylococcus aureus* biofilms release leukocidins to elicit extracellular trap formation and evade neutrophil-mediated killing. *Proc. Natl. Acad. Sci. U.S.A.* **115**, 7416–7421 (2018).
14. N. Høiby, T. Bjarnsholt, M. Givskov, S. Molin, O. Ciofu, Antibiotic resistance of bacterial biofilms. *Int. J. Antimicrob. Agents* **35**, 322–332 (2010).
15. P. S. Stewart, J. W. Costerton, Antibiotic resistance of bacteria in biofilms. *Lancet* **358**, 135–138 (2001).
16. W. H. DePas *et al.*, Biofilm formation protects *Escherichia coli* against killing by *Caenorhabditis elegans* and *Myxococcus xanthus*. *Appl. Environ. Microbiol.* **80**, 7079–7087 (2014).
17. U. Römling *et al.*, Microbial biofilm formation: A need to act. *J. Intern. Med.* **276**, 98–110 (2014).
18. T. Bjarnsholt, The role of bacterial biofilms in chronic infections. *APMIS Suppl.* **136**, 1–51 (2013).
19. S. E. Cramton, C. Gerke, N. F. Schnell, W. W. Nichols, F. Gotz, The intercellular adhesion (ica) locus is present in *Staphylococcus aureus* and is required for biofilm formation. *Infect. Immun.* **67**, 5427–5433 (1999).
20. F. Fitzpatrick, H. Humphreys, J. P. O'Gara, Evidence for icaADBC-independent biofilm development mechanism in methicillin-resistant *Staphylococcus aureus* clinical isolates. *J. Clin. Microbiol.* **43**, 1973–1976 (2005).
21. H. McCarthy *et al.*, Methicillin resistance and the biofilm phenotype in *Staphylococcus aureus*. *Front. Cell. Infect. Microbiol.* **5**, 125791 (2015).
22. S. Mishra, A. R. Horswill, Heparin mimics extracellular DNA in binding to cell surface-localized proteins and promoting *Staphylococcus aureus* biofilm formation. *mSphere* **2**, e00135-17 (2017).
23. J. B. Kaplan, A. R. Horswill, Micrococcal nuclease regulates biofilm formation and dispersal in methicillin-resistant *Staphylococcus aureus* USA300. *mSphere* **9**, e0012624 (2024).
24. J. S. Kavanaugh *et al.*, Identification of extracellular DNA-binding proteins in the biofilm matrix. *mBio* **10**, e01137-19 (2019).
25. A. S. DeFrancesco *et al.*, Genome-wide screen for genes involved in eDNA release during biofilm formation by *Staphylococcus aureus*. *Proc. Natl. Acad. Sci. USA* **114**, E5969–E5978 (2017).
26. B. R. Boles, A. R. Horswill, Agr-mediated dispersal of *Staphylococcus aureus* biofilms. *PLoS Pathog.* **4**, e1000052 (2008).
27. B. Wang, T. W. Muir, Regulation of virulence in *Staphylococcus aureus*: Molecular mechanisms and remaining puzzles. *Cell Chem. Biol.* **23**, 214–224 (2016).
28. S. K. Srivastava, K. Rajasree, A. Fasim, G. Arakere, B. Gopal, Influence of the AgrC–AgrA complex on the response time of *Staphylococcus aureus* quorum sensing. *J. Bacteriol.* **196**, 2876–2888 (2014).
29. B. Wang, A. Zhao, R. P. Novick, T. W. Muir, Activation and inhibition of the receptor histidine kinase AgrC occurs through opposite helical transduction motions. *Mol. Cell* **53**, 929–940 (2014).
30. T. Maira-Litrán *et al.*, Immunochemical properties of the Staphylococcal poly-N-acetylglucosamine surface polysaccharide. *Infect. Immun.* **70**, 4433–4440 (2002).
31. E. S. Duthie, L. L. Lorenz, Staphylococcal coagulase: Mode of action and antigenicity. *Microbiology (Reading, Engl)* **6**, 95–107 (1952).
32. J. M. Voyich *et al.*, Insights into mechanisms used by *Staphylococcus aureus* to avoid destruction by human neutrophils. *J. Immunol.* **175**, 3907–3919 (2005).
33. A. J. O'Neill, *Staphylococcus aureus* SH1000 and 8325-4: Comparative genome sequences of key laboratory strains in staphylococcal research. *Lett. Appl. Microbiol.* **51**, 358–361 (2010).
34. S. Herbert *et al.*, Repair of global regulators in *Staphylococcus aureus* 8325 and comparative analysis with other clinical isolates. *Infect. Immun.* **78**, 2877–2889 (2010).
35. K. K. Jefferson, S. E. Cramton, F. Götz, G. B. Pier, Identification of a 5-nucleotide sequence that controls expression of the ica locus in *Staphylococcus aureus* and characterization of the DNA-binding properties of IcaR. *Mol. Microbiol.* **48**, 889–899 (2003).
36. C. A. Kellenberger, C. Chen, A. T. Whiteley, D. A. Portnoy, M. C. Hammond, RNA-based fluorescent biosensors for live cell imaging of second messenger cyclic di-AMP. *J. Am. Chem. Soc.* **137**, 6432–6435 (2015).
37. M. Ender, B. Berger-Bächi, N. McCallum, A novel DNA-binding protein modulating methicillin resistance in *Staphylococcus aureus*. *BMC Microbiol.* **9**, 15–11 (2009).
38. N. McCallum, J. Hinds, M. Ender, B. Berger-Bächi, P. Stutzmann Meier, Transcriptional profiling of XdrA, a new regulator of spa transcription in *Staphylococcus aureus*. *J. Bacteriol.* **192**, 5151–5164 (2010).
39. G. Ji, R. Beavis, R. P. Novick, Bacterial interference caused by autoinducing peptide variants. *Science* **276**, 2027–2030 (1997).
40. R. L. Koenig, J. L. Ray, S. J. Maleki, M. S. Smeltzer, B. K. Hurlburt, *Staphylococcus aureus* AgrA binding to the RNAIII-agr regulatory region. *J. Bacteriol.* **186**, 7549–7555 (2004).
41. C. Vuong, H. L. Saenz, F. Gotz, M. Otto, Impact of the agr quorum-sensing system on adherence to polystyrene in *Staphylococcus aureus*. *J. Infect. Dis.* **182**, 1688–1693 (2000).
42. K. E. Beenken, J. S. Blevins, M. S. Smeltzer, Mutation of sarA in *Staphylococcus aureus* limits biofilm formation. *Infect. Immun.* **71**, 4206–4211 (2003).
43. R. P. Novick, E. Geisinger, Quorum sensing in Staphylococci. *Annu. Rev. Genet.* **42**, 541–564 (2008).
44. G. Ji, R. C. Beavis, R. P. Novick, Cell density control of Staphylococcal virulence mediated by an octapeptide pheromone. *Proc. Natl. Acad. Sci. U.S.A.* **92**, 12055–12059 (1995).
45. F. Wang *et al.*, Structural and biochemical characterization of the catalytic domains of GdpP reveals a unified hydrolysis mechanism for the DHH/DHHA1 phosphodiesterase. *Biochem. J.* **475**, 191–205 (2018).
46. J. Gundlach, F. M. Commichau, J. Stülke, Perspective of ions and messengers: An intricate link between potassium, glutamate, and cyclic di-AMP. *Curr. Genet.* **64**, 191–195 (2017).
47. A. E. Mattingly, A. A. Weaver, A. Dimkovikj, J. D. Shrout, Assessing travel conditions: Environmental and host influences on bacterial surface motility. *J. Bacteriol.* **200**, 4047 (2018).
48. M. S. Zeden *et al.*, Cyclic di-adenosine monophosphate (c-di-AMP) is required for osmotic regulation in *Staphylococcus aureus* but dispensable for viability in anaerobic conditions. *J. Biol. Chem.* **293**, 3180–3200 (2018).
49. F. M. Commichau, J. Stülke, Coping with an essential poison: A genetic suppressor analysis corroborates a key function of c-di-AMP in controlling potassium ion homeostasis in Gram-positive bacteria. *J. Bacteriol.* **200**, 562 (2018).
50. J. Gundlach *et al.*, Control of potassium homeostasis is an essential function of the second messenger cyclic di-AMP in *Bacillus subtilis*. *Sci. Signal.* **10**, eaal3011 (2017).
51. I. M. Quintana *et al.*, The KupA and KupB proteins of *Lactococcus lactis* IL1403 are novel c-di-AMP receptor proteins responsible for potassium uptake. *J. Bacteriol.* **201**, 293 (2019).
52. L. Devaux *et al.*, Cyclic di-AMP regulation of osmotic homeostasis is essential in Group B Streptococcus. *PLoS Genet.* **14**, e1007342 (2018).
53. C. F. Schuster *et al.*, The second messenger c-di-AMP inhibits the osmolyte uptake system OpuC in *Staphylococcus aureus*. *Sci. Signal.* **9**, ra81 (2016).
54. T. N. Huynh *et al.*, Cyclic di-AMP targets the cystathionine beta-synthase domain of the osmolyte transporter OpuC. *Mol. Microbiol.* **102**, 233–243 (2016).
55. R. Rocha, C. M. Teixeira-Duarte, J. M. P. Jorge, J. H. Morais-Cabral, Characterization of the molecular properties of KtrC, a second RCK domain that regulates a Ktr channel in *Bacillus subtilis*. *J. Struct. Biol.* **205**, 34–43 (2019).
56. J. A. Moscoso *et al.*, Binding of cyclic di-AMP to the *Staphylococcus aureus* sensor kinase KdpD occurs via the universal stress protein domain and downregulates the expression of the Kdp potassium transporter. *J. Bacteriol.* **198**, 98–110 (2015).
57. F. M. Commichau, J. Gibhardt, S. Halbedel, J. Gundlach, J. Stülke, A delicate connection: c-di-AMP affects cell integrity by controlling osmolyte transport. *Trends Microbiol.* **26**, 175–185 (2018).
58. A. T. Whiteley *et al.*, c-di-AMP modulates *Listeria* monocytogenes central metabolism to regulate growth, antibiotic resistance and osmoregulation. *Mol. Microbiol.* **104**, 212–233 (2017).
59. R. P. Novick *et al.*, The agr P2 operon: An autocatalytic sensory transduction system in *Staphylococcus aureus*. *Mol. Gen. Genet.* **248**, 446–458 (1995).
60. S. Periasamy *et al.*, How *Staphylococcus aureus* biofilms develop their characteristic structure. *Proc. Natl. Acad. Sci. U.S.A.* **109**, 1281–1286 (2012).
61. K. Schwartz, A. K. Syed, R. E. Stephenson, A. H. Rickard, B. R. Boles, Functional amyloids composed of phenol soluble modulins stabilize *Staphylococcus aureus* biofilms. *PLoS Pathog.* **8**, e1002744 (2012).
62. L. Bowman, M. S. Zeden, C. F. Schuster, V. Kaever, A. Gründling, New insights into the cyclic di-adenosine monophosphate (c-di-AMP) degradation pathway and the requirement of the cyclic dinucleotide for acid stress resistance in *Staphylococcus aureus*. *J. Biol. Chem.* **291**, 26970–26986 (2016).
63. R. M. Corrigan, L. Bowman, A. R. Willis, V. Kaever, A. Gründling, Cross-talk between two nucleotide-signaling pathways in *Staphylococcus aureus*. *J. Biol. Chem.* **290**, 5826–5839 (2015).
64. Y. Zhang, E. Zborníková, D. Rejman, K. Gerdes, Novel (p)ppGpp binding and metabolizing proteins of *Escherichia coli*. *mBio* **9**, e02188-17 (2018).
65. A. C. Nolan *et al.*, Purine nucleosides interfere with c-di-AMP levels and act as adjuvants to re-sensitize MRSA to β-lactam antibiotics. *mBio* **14**, e0247822 (2023).
66. J. W. Costerton, P. S. Stewart, E. P. Greenberg, Bacterial biofilms: A common cause of persistent infections. *Science* **284**, 1318–1322 (1999).
67. M. F. Moore, Biofilms, their role and treatment options in the chronic non-healing wound. *Surg. Technol. Int.* **31**, sti31/916 (2017), http://eutils.ncbi.nlm.nih.gov/entrez/eutils/elink.fcgi?dbfrom=pubmed&id=29316594&retmode=ref&cmd=prlinks.
68. R. D. Wolcott *et al.*, Chronic wounds and the medical biofilm paradigm. *J. Wound Care* 19, 45–53 (2010).
69. G. Koch *et al.*, Evolution of resistance to a last-resort antibiotic in *Staphylococcus aureus* via bacterial competition. *Cell* **158**, 1060–1071 (2014).
70. M. Otto, Critical assessment of the prospects of quorum-quenching therapy for *Staphylococcus aureus* infection. *Int. J. Mol. Sci.* **24**, 4025 (2023).
71. L.-Y. Zhou, Y. Zhu, Y.-R. Jiang, X.-J. Zhao, D. Guo, Design, synthesis and biological evaluation of dual acetylcholinesterase and phosphodiesterase 5A inhibitors in treatment for Alzheimer's disease. *Bioorg. Med. Chem. Lett.* **27**, 4180–4184 (2017).
72. S. Maehara *et al.*, Pharmacological characterization of a novel potent, selective, and orally active phosphodiesterase 2A inhibitor, PDM-631. *Eur. J. Pharmacol.* **811**, 110–116 (2017).
73. A. Abusnina, C. Lugnier, Therapeutic potentials of natural compounds acting on cyclic nucleotide phosphodiesterase families. *Cell Signal* **39**, 55–65 (2017).